www.czasopisma.pan.pl PAN www.journals.pan.pl
Chemical and Process Engineering 2019, 40 (1), 49–55
DOI: 10.24425/cpe.2018.124996

Analysis of wake structures in bubbly flows using Particle Image Velocimetry (PIV)

Björn Lewandowski[1,2*], Micha Fertig[2], Georg Krekel[2], Mathias Ulbricht[1]

[1] Chair of Technical Chemistry II, University of Duisburg-Essen, Essen, DE

[2] Faculty of Chemistry, Niederrhein University of Applied Sciences, Krefeld, DE

The flow structure around rising single air bubbles in water and their characteristics, such as equivalent diameter, rising velocity and shape, was investigated using Particle Image Velocimetry (PIV) and Shadowgraphy in a transparent apparatus with a volume of 120 mL. The effect of different volumetric gas flow rates, ranging from 4 μL/min to 2 mL/min on the liquid velocity was studied. Ellipsoidal bubbles were observed with a rising velocity of 0.25–0.29 m/s. It was found that a Kármán vortex street existed behind the rising bubbles. Furthermore, the wake region expanded with increasing volumetric gas flow rate as well as the number and size of the vortices.

Keywords: bubbly flow, Particle Image Velocimetry, wake analysis, flow characteristics, high-speed imaging

1. INTRODUCTION

Multiphase gaseous-liquid flows play an important role in the chemical industry, e.g. in bubble column reactors (Kraume, 2012). A detailed insight into flow patterns and rising velocities is possible with optical methods, like PIV (Rafiei et al., 2011). Their application to multiphase flows is, however, challenging due to the presence of different phases and complex flow structures. In particular, unwanted reflections of irradiated light at the phase boundaries complicate the analysis. Furthermore, shadow regions appear due to light refraction and reflection, so that some information is lost. Additionally, illuminated particles behind the rising bubbles are captured due to the transparency of the gaseous phase (see Fig. 1). Such particles will also be considered in the analysis, if the images are used untreated, and thus lead to invalid vectors.

Many researchers have already investigated the flow field around and the wake structures of single bubbles as well as bubble swarms (Brücker, 2000; Bröder, 2003; Sommerfeld, 2004; Liu et al., 2005; Liu and Zheng, 2006; Kim et al., 2010). Still, some controversial reports about the wake structure of bubbles are present in literature (Brücker, 1999). Reasons for this may be different purities of the water used, which has a significant influence on the bubble boundary and thus on the bubble movement itself (Sam et al., 1996; Saito et al., 2010; Li et al., 2012). Furthermore, two bubbles rising within a very short time interval tend to interact with each other, which has also a great impact on the bubble characteristics and therefore on the wake structure (Brücker, 1999). For this reason a bubble frequency of less than 80 bubbles per minute

* Corresponding author, e-mail: Bjoern.Lewandowski@hs-niederrhein.de

Reprinted with permission in an extended form from the EYEC Monograph accompanying 7th European Young Engineers Conference. *http://journals.pan.pl/dlibra/journal/98834*

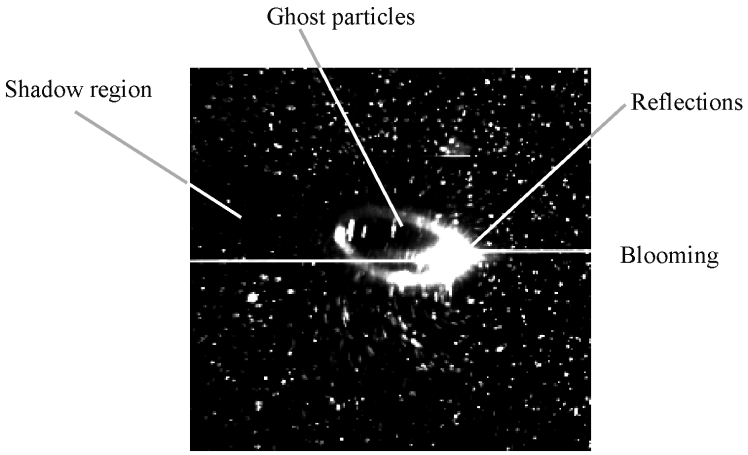

Fig. 1. Problems of multiphase PIV (Brücker, 2000)

was proposed by (Sam et al., 1996) to reduce the interaction of two consecutive bubbles (Saito et al., 2010; Rafiei et al., 2011).

2. MATERIALS AND METHODS

Air bubbles were filmed rising in deionized water in a transparent apparatus made of three millimetre thick poly(methyl methacrylate) (PMMA) plates. A schematic drawing of the experimental setup is given in Fig. 2.

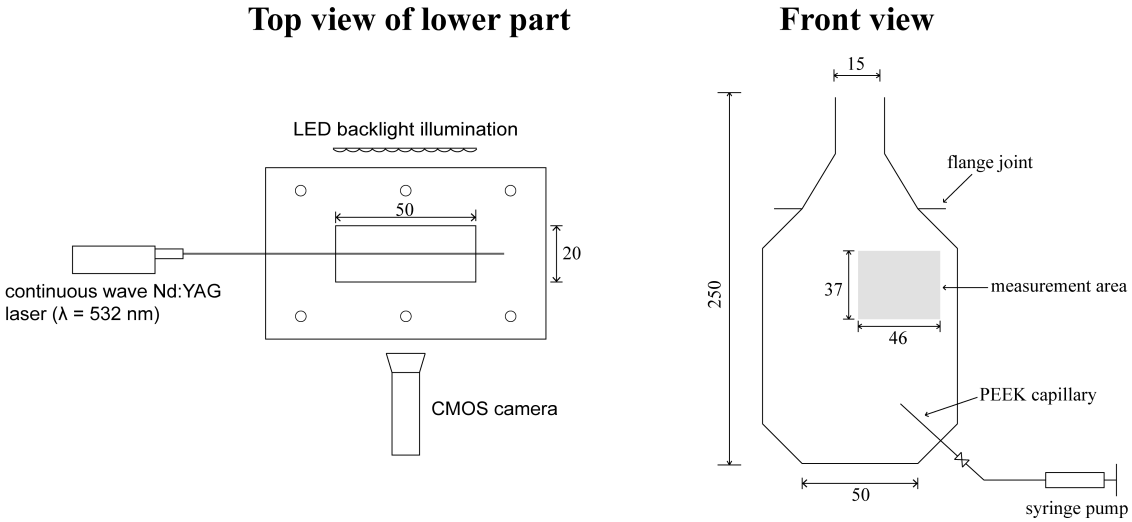

Fig. 2. Experimental setup for PIV experiments (all dimensions in mm)

A continuous wave (c.w.) Nd:YAG laser with a wave length of 532 nm and a maximum power output of 5 W (supplier: Dantec Dynamics) was used to illuminate the flow. A high-speed CMOS camera (type: Olympus iSpeed TR) with a 12× zoom lens with F-Mount (supplier: Navitar) in combination with a 0.5× lens attachment (supplier: Navitar) was used as optical system. High-speed monochrome 8 bit grayscale image sequences were captured at a frame rate of 300 fps. Thus, approx. 36 images were obtained for each bubble. The image resolution was 1280 × 1040 px. In addition to the c.w. laser, a LED backlight illumination (supplier: Dantec Dynamics) with 55,000 lux at continuous illumination mode was used to obtain Shadowgraphy images for the determination of bubble characteristics, such as equivalent diameter d_B, rising velocity w_B and elongation f_e as morphological parameter.

The equivalent bubble diameter was calculated under the assumption of rotational symmetry using the maximum and minimum axes of a fitted ellipse (Grau and Heiskanen, 2002):

$$d_B = \left(d_{\max}^2 \cdot d_{\min}\right)^{1/3} \tag{1}$$

Elongation was calculated using Equation (2). Its domain ranges from 0 for a perfect circle to 1 for an infinite line (= infinitely stretched bubble):

$$f_e = 1 - \frac{d_{\min}}{d_{\max}} \tag{2}$$

The conditions for the conducted experiments are given in Table 1. A poly(ether ether ketone) (PEEK) capillary with an internal diameter of 250 µm (supplier: Techlab) was introduced into the apparatus at the bottom at an angle of 45°. The capillary was connected to a 5 mL gastight syringe (supplier: Hamilton) filled with ambient air in a syringe pump (type: KDS 200, supplier: Cole-Parmer). Deionized water (in-house purification system, conductivity $\kappa = 17$ µS/cm) was used as liquid. The water was first degassed at 50 mbar for approx. 15 minutes before filling the apparatus. This procedure reduced the amount of unwanted gas bubbles attached to the PMMA surface in the measurement area. Polyamide seeding particles with a mean diameter of 20 µm (supplier: LaVision) were added to the water, so that at least 10 particles were present per interrogation area.

Table 1. Experimental conditions

Test conditions:	
Internal capillary diameter d_i [µm]	250
Volumetric gas flow rates $\dot{V}_g$ [mL/min]	0.004, 0.050, 2.000
Position of measurement area above capillary [mm]	60
Environmental temperature [°C]	22
Air properties (Span, 2010):	
Dynamic viscosity η_g [mPa·s]	0.0183
Density ρ_g [kg/m^3]	1.18
Water properties (Wagner and Kretzschmar, 2010):	
Dynamic viscosity η_l [mPa·s]	0.957
Density ρ_l [kg/m^3]	997.75
Surface tension γ_{lg} [N/m]	0.072

The image sequences were analysed using the adaptive correlation in Dynamic Studio v4.00 (supplier: Dantec Dynamics). The size of the interrogation area was set to 16×16 pixel, which corresponds to 0.6×0.6 mm^2, with an overlap of 25%. A peak validation with a factor of 0.5, a neighbourhood size of 5×5 pixel and an acceptance factor of 0.20 were applied for the vector validation. The liquid velocity w is calculated using the scalar map function, with U as velocity in horizontal x and V as velocity in vertical y direction:

$$w = \sqrt{U^2 + V^2} \tag{3}$$

The vorticity is analysed as a measure of the vortex strength. Since only planar PIV images are present in this work, only the rotation around the out-of-plane z axis ω_z is determined. The local velocities ∂V and ∂U are differentiated with respect to the location ∂x and ∂y, respectively:

$$\omega_z = \frac{\partial V}{\partial x} - \frac{\partial U}{\partial y} \tag{4}$$

3. RESULTS AND DISCUSSION

For the characterisation of the rising bubbles, a set of dimensionless numbers is used (Clift et al., 1978; Fan and Tsuchiya, 1990). These are the bubble Reynolds number *Re*:

$$Re = \frac{w_B \cdot d_B \cdot \varrho_l}{\eta_l} \tag{5}$$

the Eötvös number *Eo*:

$$Eo = \frac{g \cdot (\varrho_l - \varrho_g) \cdot d_B^2}{\gamma_{lg}} \tag{6}$$

and the Morton number *M* as a description for the physical properties of the fluid:

$$M = \frac{g \cdot (\varrho_l - \varrho_g) \cdot \eta_l^4}{\varrho_l^2 \cdot \gamma_{lg}^3} \tag{7}$$

The results for the bubble characteristics are given in Table 2. The standard deviations are with less than 3% negligible and therefore not listed in the table. From Table 2 it can be concluded that with an increase of $\dot{V}_g$ the bubble diameter increases from 2.53 to 2.70 mm. The same applies to the rising velocity, which increases from 0.25 to 0.29 m/s, and the elongation, which increases from 0.26 to 0.36. The measured rising velocity is in accordance with literature data from (Clift et al., 1978) for a pure water system (Clift et al., 1978). The bubble Reynolds number varied in a range of 659 to 809, the Eötvös number varied from 0.86 to 0.98 and the Morton number was constant at 2.14×10^{-11}. According to bubble shape maps found in literature, the observed bubbles are in the ellipsoidal regime (Clift et al., 1978; Fan and Tsuchiya, 1990). This is in consensus with the visual impression gained from the image sequences as well as the determined elongation (compare Table 2).

Table 2. Experimental conditions

$\dot{V}_g$ [mL/min]	d_B [mm]	w_B [m/s]	f_e [–]	*Re* [–]	*Eo* [–]	*M* [–]
0.004	2.53	0.25	0.26	659	0.86	2.14×10^{-11}
0.050	2.55	0.29	0.34	762	0.87	2.14×10^{-11}
2.000	2.70	0.29	0.36	809	0.98	2.14×10^{-11}

A typical resulting vector plot for the data analysis is given in Fig. 3. The wake structure behind the bubbles can clearly be identified. Alternating clockwise and anti-clockwise vortices can be seen, representing a typical Kármán vortex street. Additionally, the typical flow structure around the bubble is presented according to other observations in literature (Clift et al., 1978). The flow in front of the bubble is directed in the same direction as the bubble trajectory, while a circulating flow is present at the sides. Behind the bubble, the flow is again directed in direction of the bubble trajectory.

The resulting velocities and vorticities for the different volumetric gas flow rates are presented in Fig. 4. At a low volumetric gas flow rate $\dot{V}_g$ of 4 µL/min, most parts of the measurement area are calmed. In the wake region far behind the rising bubble, velocities of about 0.015 m/s can be observed. Directly behind the bubble, higher velocities of approx. 0.035 m/s were measured. The vorticity plot shows alternating clockwise (indicated in white) and anti-clockwise (indicated in black) vortices according to a Kármán vortex street. The vortices are not located in the region directly behind the bubble, but at a certain distance. The amount and size of clockwise vortices is dominant.

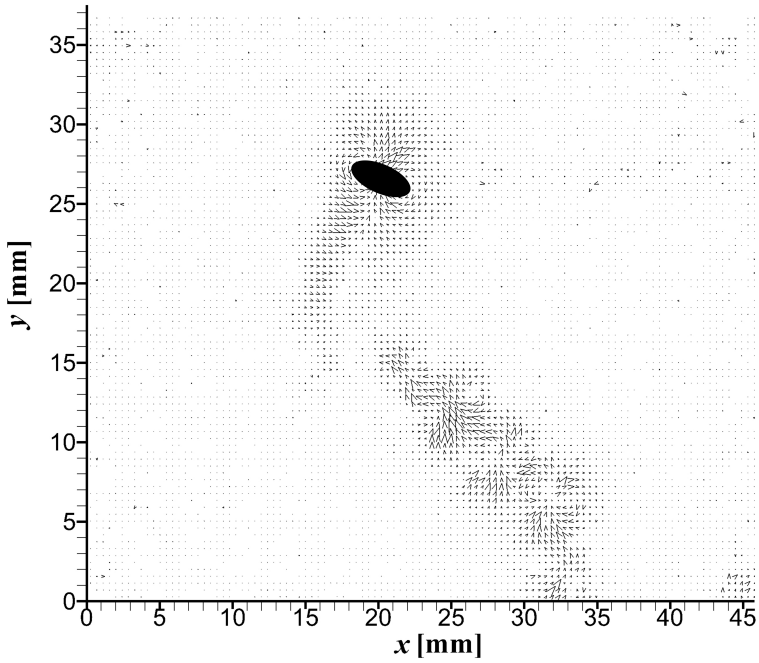

Fig. 3. Resulting vector plot for a rising bubble 117 ms after entering the measurement area (bubble position indicated as black ellipse)

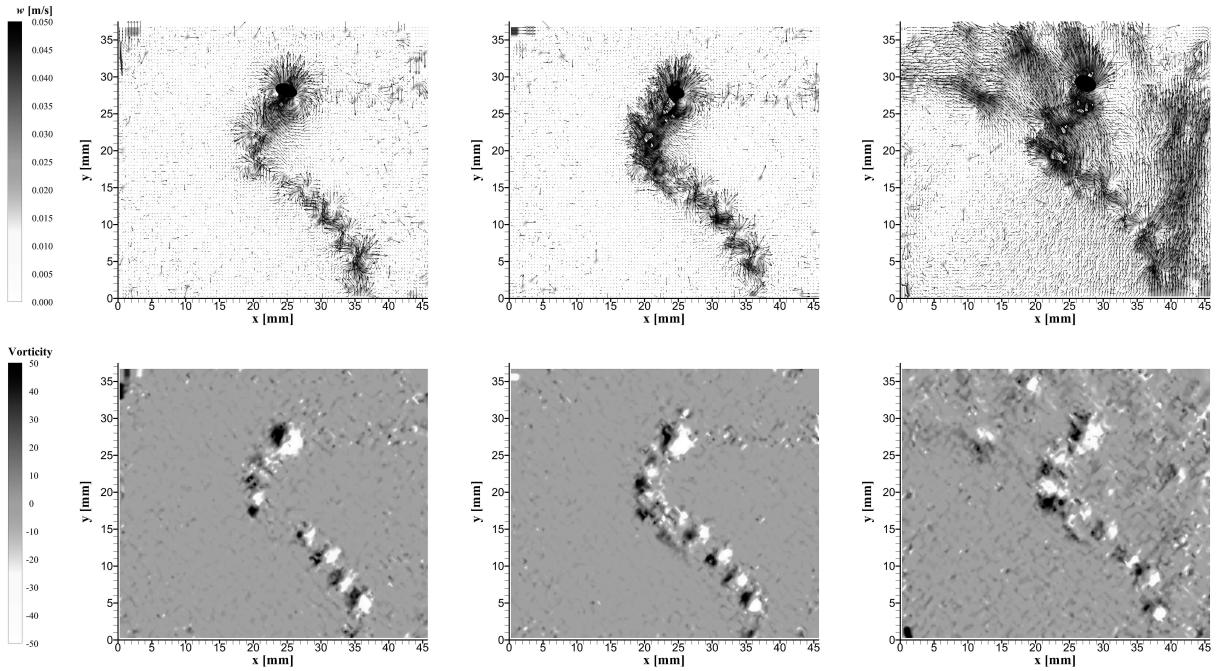

Fig. 4. Liquid velocity (top) and liquid vorticity (bottom) for volumetric gas flow rates $\dot{V}_{\mathbf{g}}$ of 4 µL/min (left), 0.05 mL/min (centre) and 2.0 mL/min (right) for rising air bubbles in deionized water 100 ms after the bubble entered the measurement area (bubble position indicated as black ellipses in velocity plots)

An increase of $\dot{V}_g$ to 0.05 mL/min leads to an expanding wake structure behind the rising bubble (see Fig. 4, centre). Furthermore, the region of higher velocities directly behind the bubble increases. The mean velocity in this area is approx. 0.045 m/s. The vorticity plot shows again a typical Kármán vortex street. The size and number of the vortices is higher than at a $\dot{V}_g$ of 4 µL/min.

Additionally, vortices can be seen in the immediate region behind the bubble. The wake structure seems more closed which is also reflected in the closed region of the wake in the velocity plot.

At $\dot{V}_g$ of 2.0 mL/min nearly 50% of the measurement area show velocities greater than zero. However, the main bubble trajectory according to the two lower volumetric gas flow rates may still be recognised in the velocity plot. A mean velocity of 0.050 m/s is present in the vicinity of the rising bubble. Furthermore, the flow seems to expand to the right-hand side and to the top left corner of the measurement area. At the right-hand side an overall downwards movement is present with some recirculating areas. These recirculation areas may be due to the small distance to the apparatus wall (compare to Fig. 2). The flow in the top left corner is mainly directed upwards due to the induced liquid velocity of the rising bubble. In the vorticity plot more regions of vortices are present than before. The amount of clockwise rotating vortices is dominant and only some anti-clockwise vortices can be identified. Compared to the vorticity plots of the other two volumetric gas flow rates, the intensity of vorticity increases.

4. CONCLUSIONS

An investigation of the bubble characteristics and wake structure of rising air bubbles in deionized water depending on the volumetric gas flow rate was carried out using optical methods such as Shadowgraphy and Particle Image Velocimetry (PIV). The bubble Reynolds number was in a range of 659 to 809 and the Eötvös number was in a range of 0.86 to 0.98 with a constant Morton number of 2.14×10^{-11}.

It was found that with increasing volumetric gas flow rate the bubbles became larger and their rising velocity increased. Furthermore, the bubbles became more ellipsoidal. Using PIV for the investigation of the flow structure it was found that the wake structure behind the rising bubbles expanded with increasing volumetric gas flow rate. Additionally, higher liquid velocities were observed in the region directly behind the bubbles. At a flow rate of 2 mL/min the flow structure included nearly the complete measurement area. Using vorticity as the representation of vortices, a Kármán vortex street with alternating clockwise and anti-clockwise rotating vortices was observed. An increase of the volumetric flow rate produced more and larger vortices. Clockwise vortices were always dominant. Additionally, recirculation areas were found at higher volumetric gas flow rates on the right-hand side of the measurement area, which may have been caused by the short distance to the apparatus wall.

SYMBOLS

CMOS	complementary metal-oxide-semiconductor
c.w.	continuous wave
d_b	equivalent bubble diameter, m
d_i	capillary internal diameter, m
Eo	Eötvös number, dimensionless
f_e	elongation, dimensionless
g	acceleration due to gravity, $m \cdot s^{-2}$
LED	light-emitting diode
M	Morton number, dimensionless
PIV	Particle Image Velocimetry
Re	bubble Reynolds number, dimensionless
U	velocity in y direction, $m \cdot s^{-1}$
V	velocity in x direction, $m \cdot s^{-1}$
$\dot{V}_g$	volumetric gas flow rate, $m^3 \cdot s^{-1}$
w	liquid velocity, $m \cdot s^{-1}$
w_B	rising velocity of bubbles, $m \cdot s^{-1}$

Greek symbols

γ_{lg}	surface tension between liquid and gaseous phase, $N \cdot m^{-1}$
η_l/η_g	dynamic viscosity of liquid/gas, Pa·s
ρ_l/ρ_g	density of liquid/gas, $kg \cdot m^{-3}$
ω_z	vorticity as rotation around z axis, s^{-1}

REFERENCES

Bröder D., 2003. *Anwendung optischer Messtechniken zur Untersuchung disperser Gas-Flüssigkeits-Strömungen*. Dissertation, Halle (Saale).

Brücker C., 1999. Structure and dynamics of the wake of bubbles and its relevance for bubble interaction. *Phys. Fluids*, 11 (7), 1781–1796. DOI: 10.1063/1.870043.

Brücker C., 2000. PIV in multiphase flows, In: Riethmuller M.L. (Ed.), *Particle Image Velocimetry and associated techniques*, *Lecture series 2000-01*. Von Karman Institute for Fluid Dynamics, Rhode Saint Genčse, Belgium: VKI.

Clift R., Grace J.R., Weber M.E., 1978. *Bubbles, drops, and particles*. 1st edition, Academic Press, New York.

Fan L., Tsuchiya K., 1990. *Bubble wake dynamics in liquids and liquid-solid suspensions*. Butterworth–Heinemann, Boston.

Grau R., Heiskanen K., 2002. Visual technique for measuring bubble size in flotation machines. *Miner. Eng.,* 15, 507–513. DOI: 10.1016/S0892-6875(02)00074-2.

Kim S.M., Yi S.J., Kim H.D., Kim J.W., Kim K.C., 2010. Dynamic analysis of bubble-driven liquid flows using time-resolved particle image velocimetry and proper orthogonal decomposition techniques. *J. Visualization*, 13, 213–220. DOI: 10.1007/s12650-010-0029-y.

Kraume M., 2012. *Transportvorgänge in der Verfahrenstechnik*. 1st ed. Springer, Berlin Heidelberg.

Li Y., Zhu T., Liu Y., Tian Y., Wang H., 2012. Effects of surfactant on bubble hydrodynamic behavior under flotation-related conditions in wastewater. *Water Sci. Technol.*, 65, 1060–1066. DOI: 10.2166/wst.2012.933.

Liu Z., Zheng Y., 2006. PIV study of bubble rising behavior. *Powder Technol.*, 168, 10–20. DOI: 10.1016/j.powtec.2006.05.020.

Liu Z., Zheng Y., Jia L., Zhang Q., 2005. Study of bubble induced flow structure using PIV. *Chem. Eng. Sci.*, 60, 3537–3552. DOI: 10.1016/j.ces.2004.03.049.

Rafiei A., Robbertze M., Finch J., 2011. Gas holdup and single bubble velocity profile. *Int. J. Miner. Process.*, 98, 89–93. DOI: 10.1016/j.minpro.2010.10.011.

Saito T., Sakakibara K., Miyamoto Y., Yamada M., 2010. A study of surfactant effects on the liquid-phase motion around a zigzagging-ascent bubble using a recursive cross-correlation PIV. *Chem. Eng. J.,* 158, 39–50. DOI: 10.1016/j.cej.2008.07.021.

Sam A., Gomez C., Finch J.A., 1996. Axial velocity profiles of single bubbles in water/frother solutions. *Int. J. Miner. Process.*, 47, 177–196. DOI: 10.1016/0301-7516(95)00088-7.

Sommerfeld M., 2004. *Bubbly flows: Analysis, modelling and calculation*. 1st edition, Springer, Berlin Heidelberg.

Span R., 2010. Properties of dry air, In: VDI-Gesellschaft Verfahrenstechnik und Chemieingenieurwesen (GVC) (Ed.), *VDI Heat Atlas*. Springer, Berlin, Heidelberg, pp. 172–191.

Wagner, W., Kretzschmar, H.-J., 2010. Properties of water and steam. in: VDI-Gesellschaft Verfahrenstechnik und Chemieingenieurwesen (GVC) (Ed.), *VDI Heat Atlas*. Springer, Berlin, Heidelberg, pp. 153–171.

Received 18 May 2018
Received in revised form 17 September 2018
Accepted 20 October 2018